Topographic Distribution of Contractile Protein in the Human Macular Microvasculature

Paula K. Yu,[1,2] Dong An,[1,2] Chandrakumar Balaratnasingam,[1,2] Stephen J. Cringle,[1,2] and Dao-Yi Yu[1,2]

[1]Centre for Ophthalmology and Visual Science, The University of Western Australia, Perth, Australia
[2]Lions Eye Institute, the University of Western Australia, Perth, Australia

Correspondence: Dao-Yi Yu, Lions Eye Institute, Centre for Ophthalmology and Visual Science, The University of Western Australia, Nedlands, West Australia, Australia 6009;
dyyu@lei.org.au.

Submitted: March 6, 2019
Accepted: September 11, 2019

Citation: Yu PK, An D, Balaratnasingam C, Cringle SJ, Yu D-Y. Topographic distribution of contractile protein in the human macular microvasculature. *Invest Ophthalmol Vis Sci*. 2019;60:4574–4582. https://doi.org/10.1167/iovs.19-26986

Purpose. We studied the topographic distribution of contractile protein in different orders of the human macular microvasculature to further understanding of the sites for capillary blood flow regulation.

Methods. Nine donor eyes from eight donors were cannulated at the central retinal artery and perfusion labeled for alpha smooth muscle actin (αSMA) and filamentous actin (F-actin). Confocal images were collected from the macula region, viewed, projected, and converted to a 255 grayscale for measurements. The mean intensity was measured for macular arterioles, venules, and capillary segments. The diameter of each vessel segment measured was recorded. The normalized mean intensity values from all images were ranked according to vessel types and size with a total of nine categories.

Results. F-actin was present throughout the macular microvasculature whereas αSMA labeling showed variations. Overall, αSMA has a more prominent presence in the macular arterioles than in the macular capillaries and venules, and αSMA strongly labeled the smaller macular arterioles. Some capillaries also labeled positive for αSMA, including some of the capillaries in the innermost capillary ring surrounding the foveola. It was weakly present in the capillaries on the venous side and larger venules. In the larger macular arterioles closer to 100 μm in diameter, αSMA labeling was weakly present and not as ubiquitous as in the smaller arterioles.

Conclusions. Nonuniform distribution of contractile proteins in the different types, orders, and sizes of macular microvasculature indicates that these vessels may have different contractile capability and roles in macular flow regulation.

Keywords: blood flow, retinal vasculature, human

The retina is one of highest metabolic-demand tissues in the human body, which is supplied by a vascular network with specific layered and plexus topography to suit the optical nature of the eye.[1–3] A critical question to be addressed is how the blood flow is regulated to meet the variation in the high metabolic demand of retinal neurons and glia.

There are remarkable differences of retinal cellular layers between the macular region and other retinal regions. Even within different areas of the macular region, structural and vascular distribution differences are significant.[4–6] Neurons have very layered topography coupled with functional and metabolic demand–specific distribution in the retina.[7] Their energy demand is significantly different in various regions and retinal layers. Even the energy demands of subcellular components within a particular cell can be different. It is a great challenge to maintain the dynamic coordination of capillary perfusion and metabolic activity. Heterogeneity of local oxygen distribution has been evidenced in many organs and tissues.[8–17] Significant heterogeneity of oxygen distribution and consumption under normal and pathologic conditions in the brain and retina have been demonstrated by our group and others.[3,12–22]

The retina is supplied by both retinal and choroidal vasculature. However, the regulation and control mechanisms for the retinal and choroidal microcirculations are quite different. The retinal microcirculation lacks autonomic innervation but has a potent local blood flow control capability.[23–25] It is important to know how the retinal microvessel network, particularly the macular microvasculature, adapts to localized metabolic demands of the functionally active neurons.[26,27] Previous studies have mainly focused on and measured the extent of autoregulation in retinal arteries over 50 μm in diameter. Increasingly, there are indications for control sites in even smaller vessels[28,29] via calcium signaling at glial endfeet[30] and perhaps also at the level of the capillaries via pericyte[31] contraction. We hypothesized that variations in the intravascular distribution of contractile proteins contributes to varied regulatory capability in various levels of the macular microvasculature. This study examines the presence and topographic distribution of contractile proteins in the macula region in human donor eyes using microcannulation and intravascular perfusion-immunofluorescence labeling techniques. We attempted to quantify the regional distribution of α-smooth muscle actin (αSMA) as it is a major contractile protein, and the amount of αSMA in a cell is thought to be proportional to the magnitude of force the cell is able to generate.[32] The αSMA distribution will be examined according to macular vessel type, order, and size. Labeling for filamentous actin was carried out at the same time for clear visualization of the entire intact retinal microvasculature.[6]

Table 1. Demographics for All Donor Eyes Included for This Study

Donor Eye	Age and Sex	Cause of Death	Postmortem Time, h
A	27 F	Bowel cancer	12
B	52 F	Subarachnoid hemorrhage secondary to aneurysm	6.5
C	55 M	Hemoptysis, cardiac arrest	20
D	60 F	Intracranial hemorrhage	6
E	60 F	Intracranial hemorrhage	6
F	62 M	Mesothelioma	24
G	64 F	Pneumonia, cardiac arrest	12
H	79 F	Motor neuron disease	12
I	90 M	Upper GI bleed	12

Materials and Methods

This study was approved by the Human Research Ethics Committee at the University of Western Australia. All human tissue was handled according to the tenets of the Declaration of Helsinki.

Human Donor Eyes

Nine donor eyes from 8 donors were used for this study. All eyes were obtained from the Lions Eye Bank of Western Australia following valid consent for use of such tissue for research purposes. Six eyes were received after the removal of corneal buttons for transplantation, and three eyes were received intact. None of the donors had a known medical history of ocular disease. The demographic data, cause of death, and the postmortem time to eye perfusion are as listed in Table 1.

Microcannulation and Perfusion Labeling

All nine eyes were cannulated at the central retinal artery, and perfusion was labeled as previously described using microcannulation and intravascular perfusion technique.[5,6]

In brief, solutions were perfused through the retinal microvasculature in the following order: Ringer's solution with 1% BSA (20 minutes), 0.1 M phosphate buffer wash (10 minutes), 10% goat serum/primary antibody (1:50 to 1:100; mouse anti-αSMA [no. A2547; Sigma-Aldrich Corp., St. Louis, MO, USA]) / 0.1% Triton X-100 (1 hour), 0.1 M phosphate buffer wash (10 minutes), 4% paraformaldehyde in 0.1 M phosphate buffer (20 minutes), 0.1 M phosphate buffer (15 minutes), secondary antibody (1:200; goat anti-mouse conjugated to Alexa Fluor 488 or 555 [A11001 and A11003, respectively; Invitrogen, City, Thermo Fisher Scientific, Waltham, MA, USA]) / Hoechst nuclei counter stain (B2261; Sigma-Aldrich Corp.) or YO-PRO-1 (Y3603; Thermo Fisher Scientific) along with phalloidin or lectin conjugated with tetramethylrhodamine or FITC (P1951 or P5282; Sigma-Aldrich) for 1 hour, followed by a final buffer wash for 30 minutes. The perfusion-labeled globes were immersed in 4% paraformaldehyde overnight for further fixation before the retinas were dissected out for flat mounting and imaging.

Confocal Imaging

Confocal images were collected from the macula region using ×4 (NA 0.20), ×10 (NA 0.45), and ×20 (NA 0.75) objective lenses at 1024 × 1024 pixel resolution (Plan Apo, Nikon C1 System; Nikon Corp., Tokyo, Japan). Confocal image stacks were collected using a set level of laser intensity and gain level. Images were viewed and projected using image analysis software (v.7.5.2, Imaris Software, Bitplane, Inc.; Zurich, Switzerland).

Vessel Categories

The arterioles are categorized by size and orders according to the modified Horton-Strahler method as described previously.[5] Macular arterioles are grouped into five categories as vessels between 60 and 100 μm (a5), 50 to 60 μm (a4), 20 to 50 μm (a3), 15 to 20 μm (a2), and those that are <15 μm in diameter (a1). Macular venules are grouped into three categories, with capillaries draining directly into venule as v1 (Table 2), those <40 μm as v2, and vessels between 40 and 60 μm as v3. All other capillaries were grouped into one category and include foveal capillaries.

Quantification

Confocal images of αSMA labeling of each region were projected and converted to 255 grayscale for measurements. The mean intensity was measured for macular arterioles, venules, and capillaries using (Image-Pro Plus v.7.0, Media Cybernetics, Inc., Silver Spring, MD, USA), whereby the outline of the vessel segment to be measured was traced and the mean intensity value obtained using the histogram tool. The diameter of each vessel segment was also measured and recorded. The intensity measurements were normalized to the highest intensity-labeled small arteriole (a3) within each image as 100% and all other measurements from the same image expressed in proportion to it. This is for ease of comparison across images and between different samples. The normalized mean intensity values from all images were ranked according to vessel types and size with a total of nine categories as detailed

Table 2. Vessel Diameter and Normalized Intensity Measurements From αSMA Label in Each Category

	Mean, μm ± SE (*n*)		
Category	Vessel Diameter	Normalized Intensity	CoV in Intensity
a5	78.69 ± 4.61 (17)	40.70% ± 7.08 (17)	0.39 ± 0.07 (17)
a4	54.86 ± 1.02 (12)	74.88% ± 9.17 (12)	0.27 ± 0.05 (12)
a3	29.46 ± 0.55 (183)	74.74% ± 2.08 (183)	0.28 ± 0.01 (183)
a2	17.28 ± 0.15 (101)	79.87% ± 4.28 (101)	0.28 ± 0.03 (101)
a1	12.48 ± 0.17 (99)	64.14% ± 5.38 (99)	0.32 ± 0.02 (99)
c	8.90 ± 0.10 (459)	64.39% ± 3.06 (459)	0.33 ± 0.02 (459)
v1	10.61 ± 0.89 (9)	59.13% ± 16.40 (9)	0.32 ± 0.03 (9)
v2	21.02 ± 1.61 (23)	50.89% ± 8.59 (23)	0.28 ± 0.04 (23)
v3	53.94 ± 4.05 (8)	26.00% ± 6.33 (8)	0.31 ± 0.10 (8)

a, macular arterioles; c, capillaries; v, macular venules; n, the number of vessels measured; SE, standard error; CoV, coefficient of variation.

Investigative Ophthalmology & Visual Science

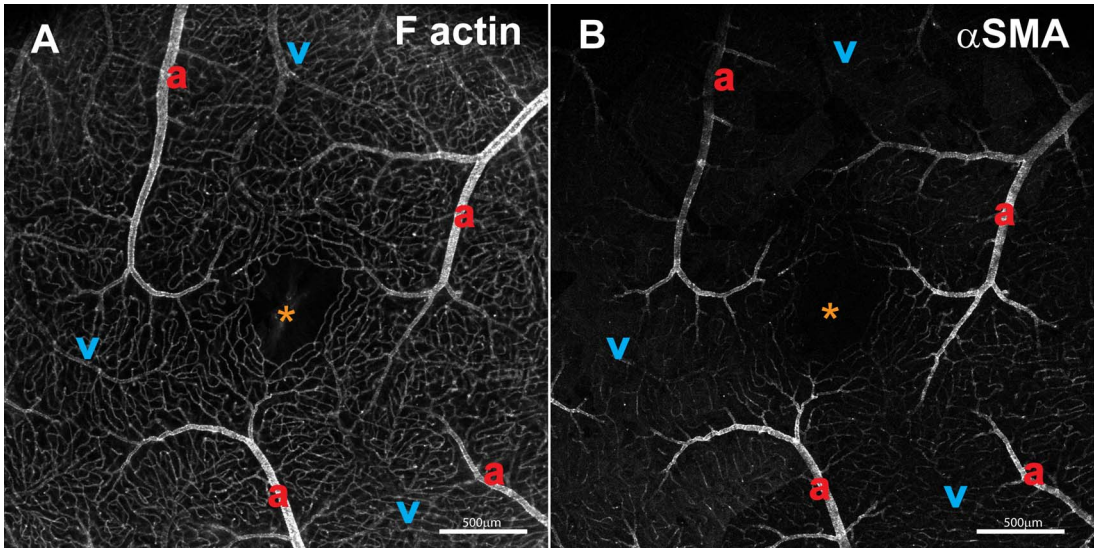

Figure 1. Low-magnification projected confocal images of the fovea region of the macula showing topographic distribution of F-actin and αSMA labeling of arterioles (a), capillaries (c), and venules (v). (**A**) All macular microvessels including arterioles, venules, and capillaries are labeled by F-actin. In general, the F-actin labeling in the venules and capillaries was weaker than in the arterioles. (**B**) αSMA labeling is present prominently in the arterioles but almost absent or very weakly present in the venules and capillaries. Small arterioles directly branching off macular arterioles also labeled strongly for αSMA, extending up to a few hundred micrometers into the vessel length. Smaller arterioles, along with some capillaries, also may be seen labeling strongly for αSMA. The venules, however, were relatively faint in the αSMA labeling and difficult to visualize at this magnification. Note that some variation in labeling intensity is present along different segments of the same order of arteriole. Weaker intensity of αSMA labeling is particularly evident in the larger size of arteriole in the top of the image. The foveolar region is indicated by an *asterisk*. *Scale bar*: 500 μm.

above. The mean and standard errors for diameter and normalized intensities were calculated for measurements within each category. The coefficient of variation was calculated for each vessel as an indication of intensity variation within each vessel segment measured.

Statistical Analysis

Data were analyzed using the R language and environment for statistical computing (https://www.R-project.org/; provided free of charge from the R Foundation for Statistical Computing, Vienna, Austria). Statistical calculations were performed using linear mixed models using eye number (identity) as the random effect to account for intraeye correlation. The labeling intensity of each vessel type was compared to v3. Eight such comparisons were performed. We used a conservative Bonferroni correction to the P value to adjust for making multiple corrections, where corrected $P = 0.05/8 = 0.0063$.

Results

Perfusion labeling of the macular microvasculature for αSMA and F-actin has been achieved in human donor eyes. The F-actin label may be seen in the cell border of endothelial cells and most strongly in the cytoplasm of vascular smooth muscle cells (vSMCs) circumferential to the major retinal arteries, whereas αSMA may be observed most strongly in the a2 to a4 vessels in the cytoplasm of vSMCs.

αSMA Distribution Qualitative

Overall, αSMA has a much stronger presence in the macular arterioles than in the macular venules. αSMA strongly labeled the vSMCs of the macular small arterioles (Figs. 1, 2). Capillaries also labeled positive for αSMA (Figs. 1–5) although not all capillaries are labeled, especially those draining into the venule side (Figs. 2, 5). αSMA is weakly present in the larger venules (Figs. 1, 2, 4) and absent from many capillaries that drain toward the venule (Fig. 5). Only some of the capillaries in the innermost ring surrounding the foveola showed positive labeling for αSMA, but all were labeled for F-actin (Fig. 5).

In the larger macular arterioles closer to 100 μm in diameter, αSMA labeling was weakly present (Figs. 1, 4) and not as ubiquitous as in the smaller arterioles.

αSMA Distribution Quantified

αSMA-labeling intensity was obtained from confocal images of eight donor eyes (eight donors). One donor eye was excluded from αSMA quantification because αSMA in donor eye A was unusual, abundantly positive in labeling the macular retinal ganglion cells and obscuring the signals from the vasculature.

Measurement of αSMA labeling intensity confirmed the qualitative observation above. The mean normalized intensity is as listed in Table 2 and plotted against each vessel category as shown in Figure 6. The vessel categories are arranged in the order of large 60- to 100-μm retinal arterioles (a5) to small arterioles less than 15 μm in diameter (a1). This is followed by capillaries, venous capillaries ~8 μm (v1), venules <40 μm (v2), and retinal venule 40 to 60 μm (v3). The category of a3 vessels encompassed a broad range of vessel diameter, from 20 to 50 μm, due to the numerous a2 vessels branching off from a3 vessels as the arteriole extend from the parafoveal through to the foveal region.

Considering the donor eye as a random factor that could have an effect on the results, a significant difference was identified between the intensity measurements between v3 vessels and those of a4, a3, a2, a1, and c ($P < 0.0063$). Vessels a1, v1, and v2 intensity measurements were not significantly different from that of v3 ($P > 0.05$). The intensity measure-

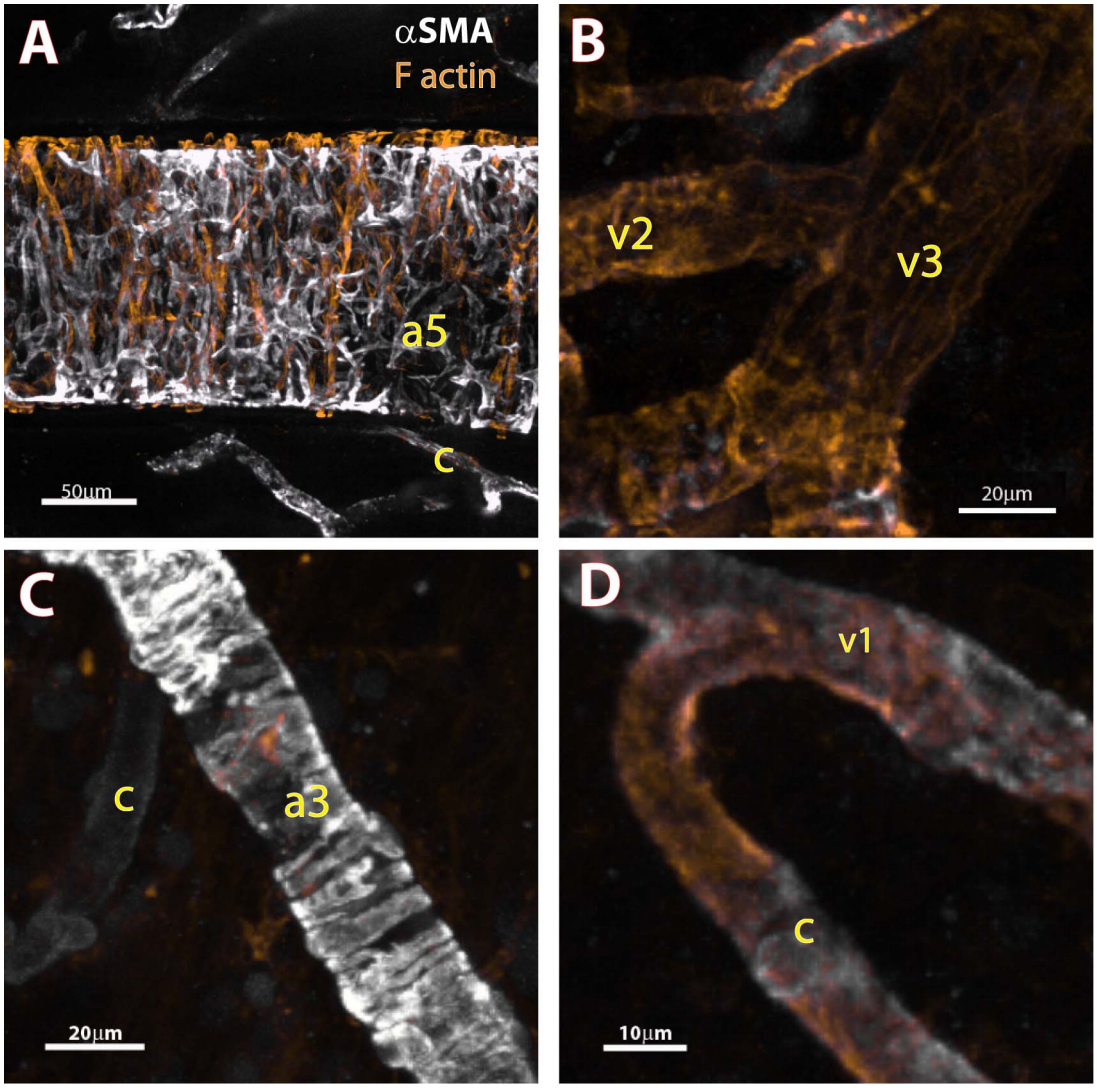

Figure 2. Confocal images of αSMA and F-actin labeling in a5 (diameter = 143 μm), a3 (diameter = 25 μm), v1 (diameter = 13.5 μm), v2 (diameter = 20 μm), v3 (diameter = 40 μm), and c (diameter = 10 to 13 μm) at higher magnifications. αSMA labeling is strongly present in the arteriole smooth muscle cells (vSMCs). Some gaps are present in the vSMC distribution along the length of the arteriole segments, likely contributing to the inconsistencies and variation in labeling intensity. v1, v2, and v3 are scarcely labeled for αSMA. The lack of positive αSMA labeling in v3 is partly due to a loss of vSMC as reflected by the concurrent lack of F-actin labeling in circumferential arrangement around the larger venules. αSMA labeling in capillaries is variable. *Scale bars*: **A** = 50 μm, **B** = 20 μm, **C** = 20 μm, **D** = 10 μm.

ments between a4, a3, a2 categories were comparable ($P > 0.7$).

The coefficient of variation (CoV) for all vessel categories range from 0.274 to 0.390, indicating a 27.4% to 39% spread of intensity measurements within each vessel category. The mean CoV and standard errors for each vessel category are listed in Table 2.

F-Actin

Six of the donor eyes were also labeled for filamentous actin using phalloidin. F-actin was labeled through all vessel levels in the macular microvasculature as previously reported.[5,33,34] A greater labeling intensity was noted in the arterioles due to the prominent presence of smooth muscle cell layers (Figs. 1, 3). All capillaries are also clearly labeled and serve as reference for the physical presence of capillaries regardless of whether αSMA labeling is positive or negative.

Discussion

In this study, we studied αSMA distribution within the macular microvasculature of human donor eyes using microperfusion and labeling techniques. This microperfusion labeling technique had been carefully evaluated and validated as published in our first paper on this topic in 2010.[6] Subsequent publications using data obtained from phalloidin and various antibody labeling of the retinal microvasculature demonstrated successful labeling of the endothelium and vSMCs in all orders of the retinal arterioles, capillaries, and venules, in both the macular and peripheral retinal microvasculature.[5,34–36] Images of the intact retinal microvasculature labeled using this microperfusion labeling technique also served as the gold standard against which images from recent advances in label-free imaging technique such as optical coherence tomography angiography may be compared for validation.[34,37–41]

Our major findings are as follows: (1) There is uneven topographic distribution of αSMA contractile proteins in the

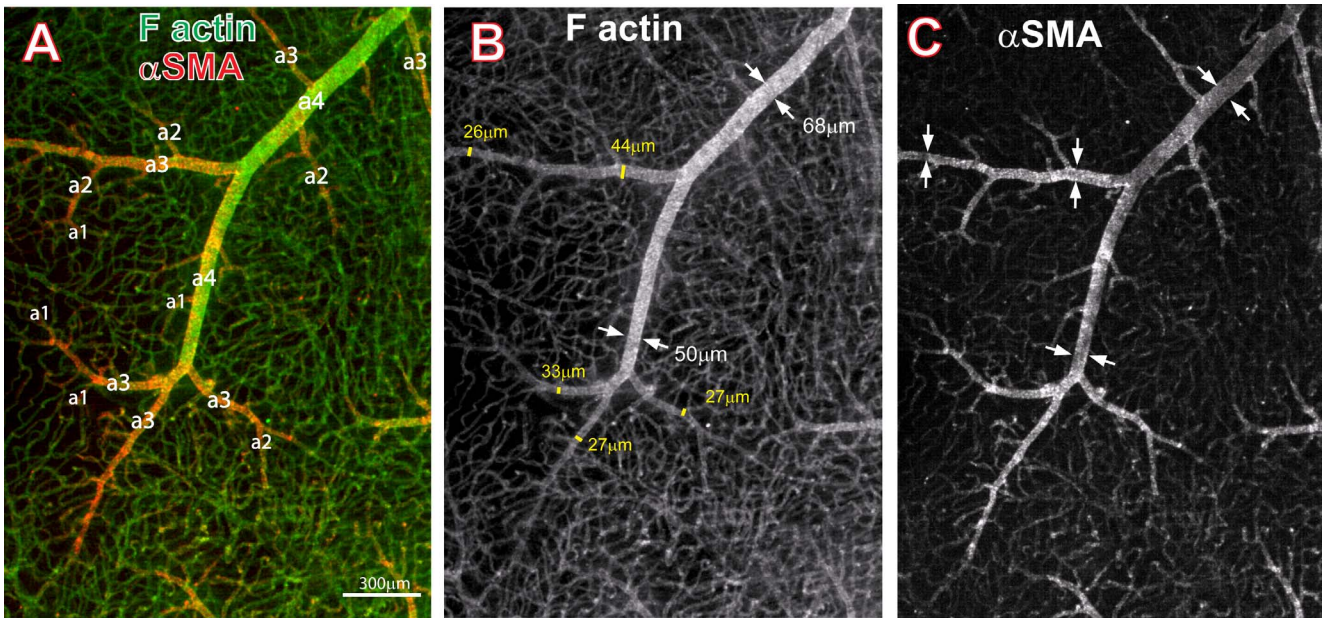

Figure 3. Higher-magnification confocal projected images of the nasal region of the macula showing F-actin and αSMA labeling of different orders of arterioles. (**A**) Dual labeling for F-actin and αSMA are shown and the macular arterioles labeled according to vessel categories of a1 to a4. Any combination of a1, a2, and a3 vessels could branch off from larger a4 arterioles. Similarly, a1and a2 arterioles could branch off a3 arterioles. The vessel widths of the same order of vessels are seen to reduce as they approached the foveola. (**B**) F-actin labeling of the macular arteriole shows fairly strong and even labeling of smooth muscle cells along the length of the a4 arteriole, which tapers from a diameter of 68 to 50 μm within this field of view. Relatively strong F-actin labeling may be seen along the a3 arterioles, which range in diameter from 27 to 44 μm for this field and also taper as they approach the foveola. (**C**) αSMA labeling is present strongly in the arterioles as well as in some capillaries. Variation in labeling intensity is present along different segments of the same order of arteriole as indicated by the pairs of *arrowheads* along the a3 and a4 vessels in this image. Weaker intensity of αSMA labeling is particularly evident in the wider portion of the a4 arteriole in the upper right corner of the image. *Scale bar*: 300 μm.

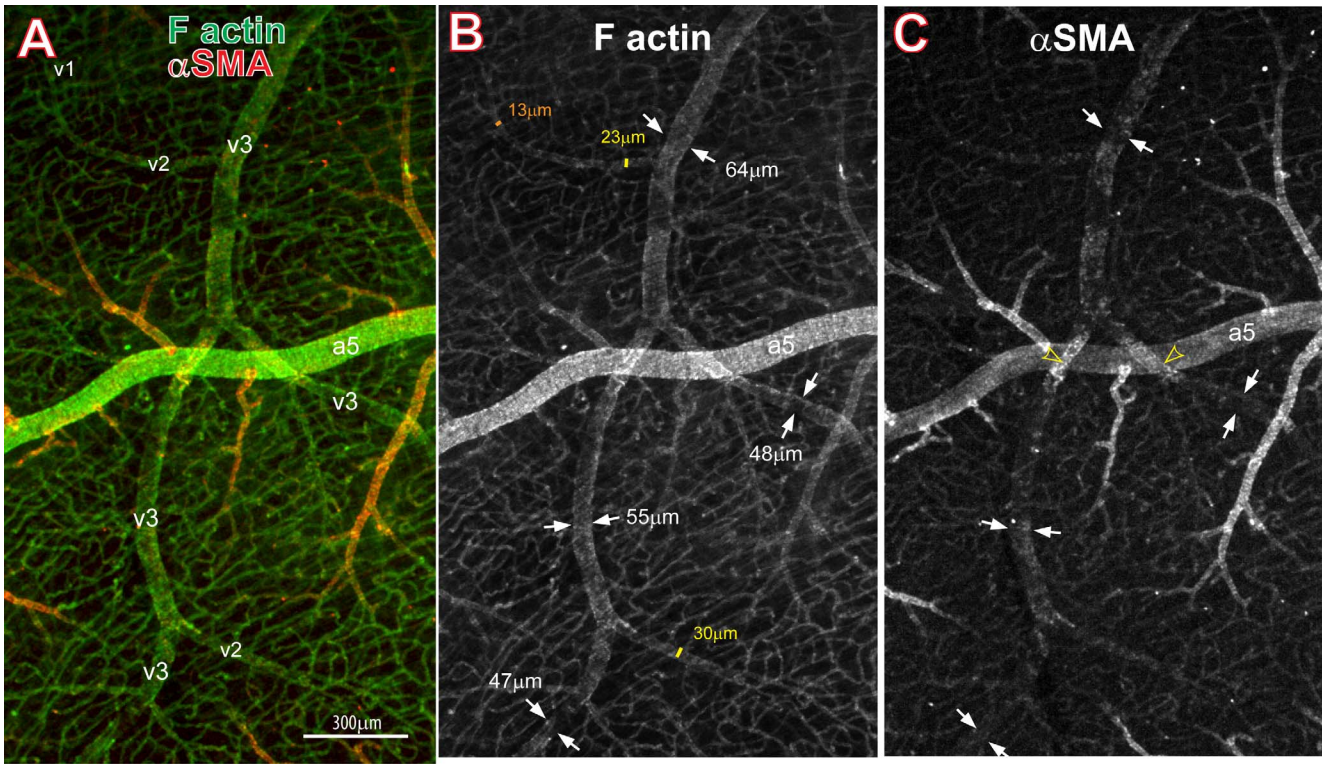

Figure 4. Higher-magnification projected confocal images of the superior region of the macula showing F-actin and αSMA labeling of different orders of venules. (**A**) Dual labeling for F-actin and αSMA are shown and the macular venule labeled according to vessel categories of v1 to v3. A larger macular arteriole (a5) may be seen running across the two venules converging. An obvious weaker labeling may be seen for both F-actin and αSMA in the venules when compared to the arterioles. (**B**) F-actin labeling of the macular venule shows relatively weak and even labeling of venule segment that broadened from 47 to 64 μm within this field of view. Even weaker F-actin labeling may be seen in v1 and v2 venules, with diameters ranging from 13 to 30 μm for this field. (**C**) αSMA labeling is present in a patchy manner in the venule and is relatively weak compared to that in the larger macular arteriole (79 μm diameter). Variation in labeling intensity is present along the entire length of this v3 venule. αSMA labeling intensity on the venule appears to be higher in the vicinity of the arteriole-venule crossing points (*yellow triangles*). *Scale bar*: 300 μm.

Investigative Ophthalmology & Visual Science

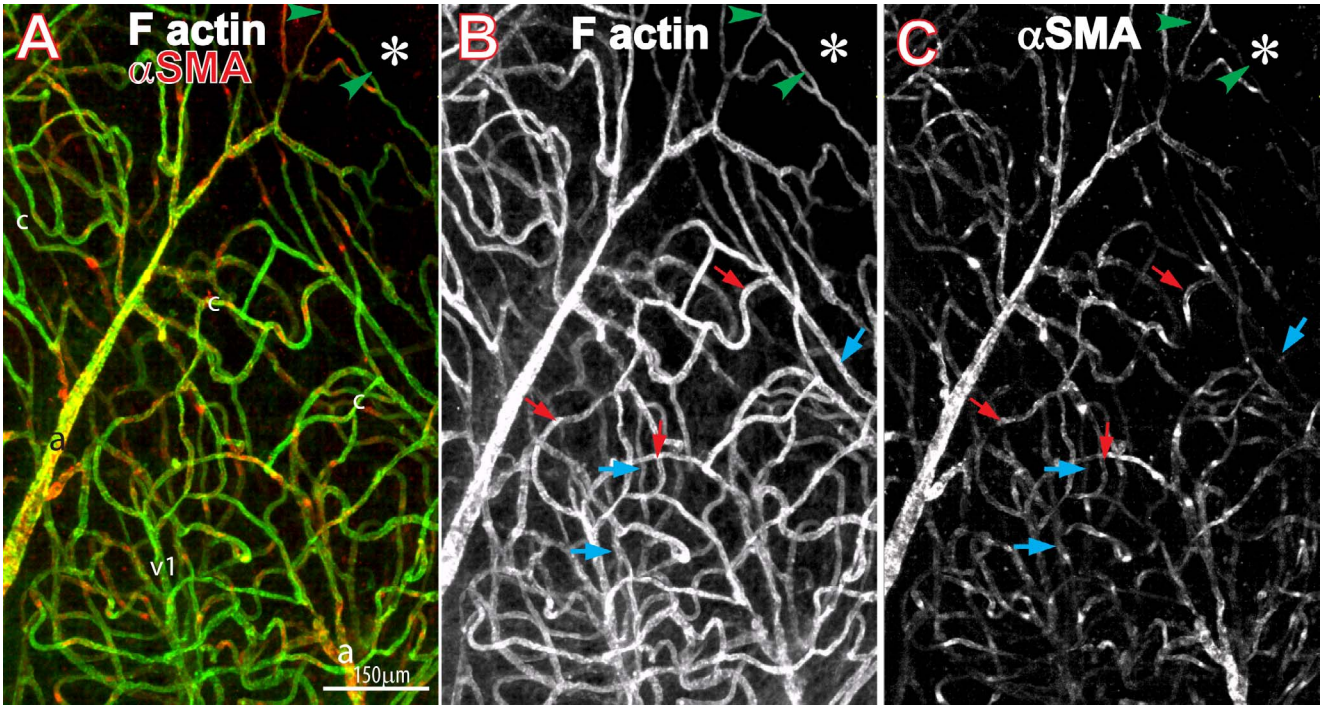

FIGURE 5. High-magnification projected image of foveal segment vasculature showing detail labeling of αSMA and F-actin at the capillary level. (**A**) Dual labeling of F-actin and αSMA in this region shows variable level of αSMA at the capillary level. Two terminal ends of the macula arterioles (a), a small macula venule (v1), and numerous interconnecting capillaries (c) may be seen in this field. Part of the foveola (*) is visible in this field. *Two green triangles* point to position of the foveal capillary ring. (**B**) F-actin labeling shows the intact and connected microvasculature. Stronger labeling was observed in the arteriole compared to the venule. Generally, F-actin labeling in capillaries is relatively even along each capillary segment but appears to be weaker on the venous side as well as at the foveal capillaries. *Solid white arrows* point to capillaries of arteriole origin and *open arr*ows point to capillaries draining toward the venous side. (**C**) αSMA labeling is strongly present in the arteriole as well as capillaries from arteriole origin (*red solid arrows*). αSMA is variably present in foveal capillaries as indicated by the *open arrowheads*. Venous capillaries tend to label weakly for αSMA (*blue arrows*). *Scale bar*: 150 μm.

macular microvasculature, with stronger expression in the arteriole and weaker in capillary and venules; (2) αSMA-labeling intensity was not always proportional to the diameter of the artery or arterioles, with the most prominent labeling found in macular arterioles less than 60 μm in diameter and rather weakly present in arterioles larger than 60 μm in diameter; (3) Capillary αSMA labeling is also uneven and partial; and (4) The level of αSMA labeling in the arterioles was not proportional to the amount of vSMCs or endothelium present, as evident from the lack of correlation between arteriole diameter and intensity measurements.

αSMA is probably the single most abundant protein in adult vSMCs. It is thought to have a central role in regulating vascular contractility and blood pressure homeostasis.[42] The location and presence of contractile proteins within the macular microvasculature is suggestive of its capability to regulate blood supply. From the data presented, it has been demonstrated that the most intensely labeled area is in macular small arterioles, suggestive of local regulatory sites for the regional and localized macular regions. This finding agrees with a recent report of rat retinal vasculature in which αSMA was high in arterioles and low in capillaries.[43] It is interesting that our results show that the most intense labeling was in arterioles 20 to 30 μm in diameter, but even arterioles with smaller caliber have a very high level of labeling for αSMA.

With respect to the distribution of blood pressure and flow in the circulation, an important consequence is the relation between flow resistance and vessel radius. The rate of blood flow is directly proportional to the fourth power of the radius of the vessels.[36] Although Poiseuille's law (Appendix) does not apply to such small vessels, a diameter change in arterioles less than 20 μm could still play a significant role in retinal capillary perfusion, not only by changing the flow resistance, but also by altering the Fahraeus-Lindqvist effect (a phenomenon describing the change in viscosity of blood with the decrease in diameter at the level of microcirculation).[36,44–47]

It has been reported that the oxygen tension in the tissues could affect the degree of opening and closing of these smallest arterioles.[48,49] Oxygen distribution in the retina is known to be significantly heterogeneous in the different retinal layers and regions such as the macula and peripheral retina.[3,19,22] Weaker αSMA labeling in large arterioles more than 60 μm in diameter may indicate a lesser regulatory capability via contraction. However, we cannot rule out that this weaker αSMA labeling is affected by aging, postmortem change, and other age-related pathologic factors in the human donor eyes. Another possible contributor could be insufficient penetration of the antibody through the thicker muscular layers of these large arterioles.

Our data also demonstrated relatively weaker αSMA labeling in the capillaries and venules when compared with small arterioles. Only partial capillaries were positively labeled in our study. It may indicate that there is some regulatory capability in the macular capillaries.

We also found that αSMA labeling in venules was weaker than that in capillaries, but was not absent. Some weak contractile capability may be suggested. In fact, we recently demonstrated that potent contractile agents such as ET-1 can induce porcine retinal vein contraction in vitro using an isolated perfused vein preparation,[50] with similar results also reported by another group.[51]

One of the most fundamental principles of blood circulation is the ability of each tissue to autoregulate its local blood flow

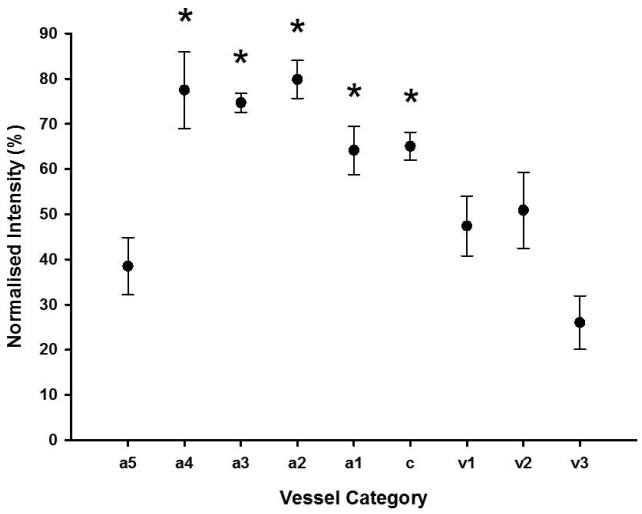

FIGURE 6. Graph showing αSMA labeling intensity level expressed as mean and standard errors in the nine categories of macular microvessels. The presence of statistically significant ($P < 0.0063$) differences in intensity measurements per vessel category compared against v3 vessel category is as marked with an *asterisk*. v3 has significantly lower intensity of αSMA labeling when compared against a4 to c categories. Vessel categories: a5 = macular arterioles 60 to 100 μm; a4 = macular arterioles 50 to 60 μm, a3 = macular arterioles 20 to 50 μm; a2 = macular arterioles 15 to 20 μm; a1= macular arterioles <15 μm; c = capillaries, v1 = capillaries draining into venous side; v2 = macular venules < 40 μm; v3 = macular venules 40 to 60 μm; * denotes $P < 0.0063$.

in proportion to its metabolic needs. The blood flow supplying each tissue is likely most optimally regulated at the level that meets the tissue's requirements. An unusual feature of the retinal circulation is the lack of autonomic innervation,[52] so more reliance must be placed on local vascular control mechanisms.[24] Local regulation is the most efficient way to provide all nutrients to meet the demands of the tissues and cells to achieve neurovascular coupling.[53] It is known that the oxygen tension in monkey fovea and some layers of the rat retina is very low, close to critical oxygen tension (~5 mm Hg) in physiological condition.[3,19,20,22,54,55] The regulatory control of blood flow in the eye is therefore a vital component in the maintenance of retinal homeostasis. In addition, local blood flow control can be divided into acute control and long-term control. For the macula, it is clear that controlling points closer to the capillary network, that is, smaller arterioles, are better placed to microadjust the capillary perfusion to best match metabolic demands of local tissue and cells rather than the larger vessels.[36] Therefore, it is understandable that small arterioles could play a major regulatory role in the macular microvasculature. The topographic distribution of αSMA labeling may indicate that different type, order, and size of macular microvessels may have different roles in the orchestrated control of local blood flow regulation.

The control mechanisms in the macular microvasculature are important for our understanding of macular physiology in normal and disease states, and it could be complicated. The results from this current study on the topographic distribution of αSMA confirmed that major local flow control points are likely to be arterioles less than 30 μm in diameter and that further study of other contractile proteins such as calponin,[56] myosin,[57] and MLCK[58] could add to our understanding of the local control mechanisms. Understanding the relationship between the expression of such contractile proteins and their function in the control of local perfusion of retinal microcompartments in normal and disease states could be the key to developing early diagnosis modality and intervention strategies.

Acknowledgments

Supported by the National Health Medical Research Council, Australia.

Disclosure: **P.K. Yu**, None; **D. An**, None; **C. Balaratnasingam**, None; **S.J. Cringle**, None; **D.-Y. Yu**, None

APPENDIX

Resistance is the impediment to blood flow in a vessel, which cannot be measured directly. But it can be calculated by measured blood flow and pressure difference between two points in a vessel. Poiseuille investigated the passage of simple fluids through long, narrow-bore tubes. His main findings can be represented by the equation, known as Poiseuille's law.[59]

$$Q = \frac{\pi \, \Delta P \, r^4}{8 \, \eta \, l}$$

This equation gives the flow (Q) through a cylindrical tube as a function of the driving pressure difference along the tube (ΔP), the tube radius (r) and length (l). The dynamic viscosity (η) is a material property of the fluid, which describes its internal resistance to shearing motions, in which different parts of the fluid move with different velocities.

References

1. Anderson B, Saltzman HA. Retinal oxygen utilization measured by hyperbaric blackout. *Arch Ophthalmol*. 1964;72:792–795.
2. Ames A. Energy requirements of CNS cells as related to their function and to their vulnerability to ischemia: a commentary based on studies on retina. *Can J Physiol Pharmacol*. 1992;70:S158–S164.
3. Yu DY, Cringle SJ. Oxygen distribution and consumption within the retina in vascularised and avascular retinas and in animal models of retinal disease. *Prog Retin Eye Res*. 2001;20:175–208.
4. Yu DY, Yu PK, Balaratnasingam C, Cringle SJ, Su EN. Microscopic structure of the retina and vasculature in the human eye. In: Méndez-Vilas A, Díaz J, eds. *Microscopy: Science, Technology, Applications and Education*. Badajoz, Spain: Formatex Research Center; 2010:867–875.
5. Yu PK, Balaratnasingam C, Cringle SJ, McAllister IL, Provis J, Yu DY. Microstructure and network organization of the microvasculature in the human macula. *Invest Ophthalmol Vis Sci*. 2010;51:6735–6743.
6. Yu PK, Balaratnasingam C, Morgan WH, Cringle SJ, McAllister IL, Yu DY. The structural relationship between the microvasculature, neurons, and glia in the human retina. *Invest Ophthalmol Vis Sci*. 2010;51:447–458.
7. Yu DY, Cringle SJ, Balaratnasingam C, Morgan WH, Yu PK, Su EN. Retinal ganglion cells: energetics, compartmentation, axonal transport, cytoskeletons and vulnerability. *Prog Retin Eye Res*. 2013;36:217–246.
8. Intaglietta M, Johnson PC, Winslow RM. Microvascular and tissue oxygen distribution. *Cardiovasc Res*. 1996;32:632–643.
9. Lubbers DW, Baumgartl H. Heterogeneities and profiles of oxygen pressure in brain and kidney as examples of the pO_2 distribution in the living tissue. *Kidney Int*. 1997;51:372–380.
10. Pittman RN. Oxygen supply to contracting skeletal muscle at the microcirculatory level: diffusion vs. convection. *Acta Physiol Scand*. 2000;168:593–602.
11. Rumsey WL, Pawlowski M, Lejavardi N, Wilson DF. Oxygen-pressure distribution in the heart in-vivo and evaluation of the ischemic border zone. *Am J Physiol*. 1994;266:H1676–H1680.

12. Ahmed J, Braun RD, Dunn R Jr, Linsenmeier RA. Oxygen distribution in the macaque retina. *Invest Ophthalmol Vis Sci*. 1993;34:516–521.
13. Acker T, Acker H. Cellular oxygen sensing need in CNS function: physiological and pathological implications. *J Exp Biol*. 2004;207:3171–3188.
14. Ames A. CNS energy metabolism as related to function. *Brain Res Rev*. 2000;34:42–68.
15. Cassot F, Lauwers F, Fouard C, Prohaska S, Lauwers-Cances V. A novel three-dimensional computer-assisted method for a quantitative study of microvascular networks of the human cerebral cortex. *Microcirculation*. 2006;13:1–18.
16. Dahlgren N, Lindvall O, Sakabe T, Stenevi U, Siesjo BK. Cerebral blood flow and oxygen consumption in the rat brain after lesions of the noradrenergic locus coeruleus system. *Brain Res*. 1981;209:11–23.
17. Feng ZC, Roberts EL Jr, Sick TJ, Rosenthal M. Depth profile of local oxygen tension and blood flow in rat cerebral cortex, white matter and hippocampus. *Brain Res*. 1988;445:280–288.
18. Cringle SJ, Yu D-Y, Yu PK, Su E-N. Intraretinal oxygen consumption in the rat in vivo [published erratum appears in *Invest Ophthalmol Vis Sci.* 2003;44:9]. *Invest Ophthalmol Vis Sci.* 2002;43:1922–1927.
19. Yu DY, Cringle SJ, Alder VA, Su EN. Intraretinal oxygen distribution in rats as a function of systemic blood pressure. *Am J Physiol*. 1994;267:H2498–H2507.
20. Yu DY, Cringle SJ, Yu PK, Su EN. Intraretinal oxygen distribution and consumption during retinal artery occlusion and graded hyperoxic ventilation in the rat. *Invest Ophthalmol Vis Sci*. 2007;48:2290–2296.
21. Linsenmeier RA, Braun RD. Oxygen distribution and consumption in the cat retina during normoxia and hypoxemia. *J Gen Physiol*. 1992;99:177–197.
22. Yu DY, Cringle SJ, Su EN. Intraretinal oxygen distribution in the monkey retina and the response to systemic hyperoxia. *Invest Ophthalmol Vis Sci*. 2005;46:4728–4733.
23. Kaufman PL, Alm A, eds. *Adler's Physiology of the Eye: Elinical Application*. St. Louis, MO: Mosby; 2003.
24. Yu DY, Su EN, Cringle SJ, Yu PK. Isolated preparations of ocular vasculature and their applications in ophthalmic research. *Prog Retin Eye Res*. 2003;22:135–169.
25. Laties AM, Jacobowitz D. A comparative study of the autonomic innervation of the eye in monkey, cat, and rabbit. *Anat Rec*. 1966;156:383–389.
26. Wong-Riley MT. Energy metabolism of the visual system. *Eye Brain*. 2010;2:99–116.
27. Yu DY, Yu PK, Cringle SJ, Kang MH, Su EN. Functional and morphological characteristics of the retinal and choroidal vasculature. *Prog Retin Eye Res*. 2014;40:53–93.
28. Kornfeld M, Gutierrez AM, Gonzalez E, Salomonsson M, Persson AEG. Cell calcium concentration in glomerular afferent and efferent arterioles under the action of noradrenaline and angiotensin II. *Acta Physiol Scand*. 1994;151:99–105.
29. Hill RA, Tong L, Yuan P, Murikinati S, Gupta S, Grutzendler J. Regional blood flow in the normal and ischemic brain is controlled by arteriolar smooth muscle cell contractility and not by capillary pericytes. *Neuron*. 2015;87:95–110.
30. Biesecker KR, Srienc AI, Shimoda AM, et al. Glial cell calcium signaling mediates capillary regulation of blood flow in the retina. *J Neurosci*. 2016;36:9435–9445.
31. Alarcon-Martinez L, Yilmaz-Ozcan S, Yemisci M, et al. Capillary pericytes express alpha-smooth muscle actin, which requires prevention of filamentous-actin depolymerization for detection. *Elife*. 2018;7:e34861.
32. Hughes S, Chan-Ling T. Characterization of smooth muscle cell and pericyte differentiation in the rat retina in vivo. *Invest Ophthalmol Vis Sci*. 2004;45:2795–2806.
33. Tan PEZ, Yu PK, Cringle SJ, Yu DY. Quantitative assessment of the human retinal microvasculature with or without vascular comorbidity. *Invest Ophthalmol Vis Sci*. 2014;55:8439–8452.
34. Yu PK, Mammo Z, Balaratnasingam C, Yu DY. Quantitative study of the macular microvasculature in human donor eyes. *Invest Ophthalmol Vis Sci*. 2018;59:108–116.
35. Yu PK, Tan PE, Morgan WH, Cringle SJ, McAllister IL, Yu DY. Age-related changes in venous endothelial phenotype at human retinal artery-vein crossing points. *Invest Ophthalmol Vis Sci*. 2012;53:1108–1116.
36. Yu DY, Cringle SJ, Yu PK, et al. Retinal capillary perfusion: spatial and temporal heterogeneity. *Prog Retin Eye Res*. 2019;70:23–54.
37. Yu PK, Balaratnasingam C, Xu J, et al. Label-free density measurements of radial peripapillary capillaries in the human retina. *PLoS One*. 2015;10:e0135151.
38. Chan G, Balaratnasingam C, Xu J, et al. In vivo optical imaging of human retinal capillary networks using speckle variance optical coherence tomography with quantitative clinicohistological correlation. *Microvasc Res*. 2015;100:32–39.
39. Mammo Z, Balaratnasingam C, Yu PK, et al. Quantitative noninvasive angiography of the fovea centralis using speckle variance optical coherence tomography. *Invest Ophthalmol Vis Sci*. 2015;56:5074–5086.
40. Tan PE, Balaratnasingam C, Xu J, et al. Quantitative comparison of retinal capillary images derived by speckle variance optical coherence tomography with histology. *Invest Ophthalmol Vis Sci*. 2015;56:3989–3996.
41. Mammo Z, Heisler M, Balaratnasingam C, et al. Quantitative optical coherence tomography angiography of radial peripapillary capillaries in glaucoma, glaucoma suspect, and normal eyes. *Am J Ophthalmol*. 2016;170:41–49.
42. Schildmeyer LA, Braun R, Taffet G, et al. Impaired vascular contractility and blood pressure homeostasis in the smooth muscle alpha-actin null mouse. *FASEB J*. 2000;14:2213–2220.
43. Kornfield TE, Newman EA. Regulation of blood flow in the retinal trilaminar vascular network. *J Neurosci*. 2014;34:11504–11513.
44. Long DS, Smith ML, Pries AR, Ley K, Damiano ER. Microviscometry reveals reduced blood viscosity and altered shear rate and shear stress profiles in microvessels after hemodilution. *Proc Natl Acad Sci U S A*. 2004;101:10060–10065.
45. Albrecht KH, Gaehtgens P, Pries A, Heuser M. The Fahraeus effect in narrow capillaries (i.d. 3.3 to 11.0 micron). *Microvasc Res*. 1979;18:33–47.
46. Pries AR, Secomb TW, Gaehtgens P, Gross JF. Blood flow in microvascular networks. Experiments and simulation. *Circ Res*. 1990;67:826–834.
47. Pries AR, Secomb TW, Gaehtgens P. Structural adaptation and stability of microvascular networks: theory and simulations. *Am J Physiol*. 1998;275:H349–H360.
48. Tsai AG, Intaglietta M. Evidence of flowmotion induced changes in local tissue oxygenation. *Int J Microcirc Clin Exp*. 1993;12:75–88.
49. Tsai AG, Johnson PC, Intaglietta M. Oxygen gradients in the microcirculation. *Physiol Rev*. 2003;83:933–963.
50. Yu DY, Su EN, Cringle SJ, Morgan WH, McAllister IL, Yu PK. Local modulation of retinal vein tone. *Invest Ophthalmol Vis Sci*. 2016;57:412–419.
51. Chen YL, Ren Y, Xu W, Rosa RH Jr, Kuo L, Hein TW. Constriction of retinal venules to endothelin-1: obligatory roles of ETA receptors, extracellular calcium entry, and rho kinase. *Invest Ophthalmol Vis Sci*. 2018;59:5167–5175.

Investigative Ophthalmology & Visual Science

52. Laties AM. Central retinal artery innervation. Absence of adrenergic innervation to the intraocular branches. *Arch Ophthalmol*. 1967;77:405–409.
53. Kur J, Newman EA, Chan-Ling T. Cellular and physiological mechanisms underlying blood flow regulation in the retina and choroid in health and disease. *Prog Retin Eye Res*. 2012; 31:377–406.
54. Cringle SJ, Yu D-Y. A multi-layer model of retinal oxygen supply and consumption helps explain the muted rise in inner retinal PO_2 during systemic hyperoxia. *Comp Biochem Physiol*. 2002;132:61–66.
55. Yu DY, Cringle SJ. Retinal degeneration and local oxygen metabolism. *Exp Eye Res*. 2005;80:745–751.
56. Rozenblum GT, Gimona M. Calponins: adaptable modular regulators of the actin cytoskeleton. *Int J Biochem Cell Biol*. 2008;40:1990–1995.
57. Wanjare M, Kusuma S, Gerecht S. Perivascular cells in blood vessel regeneration. *Biotechnol J*. 2013;8:434–447.
58. Martinsen A, Schakman O, Yerna X, Dessy C, Morel N. Myosin light chain kinase controls voltage-dependent calcium channels in vascular smooth muscle. *Pflugers Arch*. 2014;466: 1377–1389.
59. Tuma RF, Duran WN, Ley K. *Handbook of Physiology: Microcirculation*. 2nd ed. San Diego: Academic Press; 2008.

Investigative Ophthalmology & Visual Science